Chemical Engineering Journal 410 (2021) 128301

Contents lists available at ScienceDirect

Chemical Engineering Journal

journal homepage: www.elsevier.com/locate/cej

Bioinspired ultrathin graphene nanosheets sandwiched between epoxy layers for high performance of anticorrosion coatings

Xiaobo Zhu [a,b,c], Haichao Zhao [a,c,*], Liping Wang [a,*], Qunji Xue [a]

[a] Key Laboratory of Marine Materials and Related Technologies, Zhejiang Key Laboratory of Marine Materials and Protective Technologies, Ningbo Institute of Materials Technology and Engineering, Chinese Academy of Sciences, Ningbo 315201, China
[b] University of Chinese Academy of Sciences, Beijing 100049, China
[c] Innovation Academy of South China Sea Ecology and Environmental Engineering, Chinese Academy of Sciences, Guangzhou 510301, China

ARTICLE INFO

Keywords:
Bioinspired design
Graphene
Dopamine
Self-alignment
Sandwich coating
Anticorrosion

ABSTRACT

The special "brick-mud" layered micro-nano structure of nacre has undergone millions of years of biological evolution, which can withstand the corrosion of seawater in different environments, and has both high strength and toughness. Inspired by mussels and natural nacre, we successfully designed a bionic epoxy-(graphene-dopamine)$_n$-epoxy sandwich composite coating. Not only does dopamine act as a binder to improve the interfacial compatibility and adhesion between epoxy resin and graphene, but due to the hydrogen bonding and the electrostatic interaction of $-COO^-$ and $-NH_3^+$, graphene interlayers is parallel to the substrate and arranged between two epoxy coatings. This not only gives full play to the barrier effect of graphene, but also shielding the galvanic corrosion by avoiding direct contacting with the substrate. The results show that the composite coating prepared 10 scanning of dopamine functionalized graphene oxide has a low-frequency impedance of 1.30×10^9 O cm^2 after immersion in 3.5 wt% NaCl solution for 90 days, which is three orders of magnitude higher than that of pure coating, revealing remarkable long-term anticorrosion. We consider that our strategy can be readily extended to the self-alignment of a variety of two-dimensional nanofillers to facilitate the development of long-term corrosion resistant coatings.

1. Introduction

Electrodeposition of aqueous organic coatings are extensively employed in the automobiles and ships owing to their advantages of environmental friendliness, high degree of automation, supernal coating utilization, and the ability to coat metal substrates with complex shapes [1]. However, during the long-term service in the harsh marine environment, corrosive media (such as H_2O, O_2, Cl^-, etc.) will have a high permeability to the organic coating, resulting in the interface peeling of the coating and the serious corrosion of the substrate [2,3]. Two dimension graphene sheets have the advantages of high aspect ratio, high specific surface area, excellent barrier properties, and can effectively inhibit the penetration and diffusion of corrosive substances [4-8]. These excellent properties have led researchers to conduct a lot of research on the potential applications of graphene in anticorrosion coatings [9-11]. Kirill I. Bolotin et al. found that graphene prepared by chemical vapor deposition (CVD) can be used as a metal protective film due to its excellent barrier properties [12]. Schriver and co-workers demonstrated that graphene films can act as effective barriers to molecules such as O_2 and H_2O [13]. However, the graphene film grown by the CVD method has many defects, which reduces the long-term corrosion resistance of the graphene film. Singh Raman and colleagues reported that it was possible to achieve long-lasting corrosion resistance to metal substrates by using multilayer graphene sheets instead of single sheet of graphene [14-16]. This is because the defects in a single graphene sheet are covered via other covering layers, further providing good corrosion protection for the metal.

Graphene can be used not only as a metal protective film directly, but also as a nano-filler additive in polymer matrix [17-19]. Chang et al. incorporated functionalized graphene into the polymer, and the results show that the addition of graphene enhances the barrier properties of the composite material and improves the anticorrosion of the coating [20]. In our previous studies, it was also reported that hydrophilic polypyrrole modified graphene nanosheets can improve the

* Corresponding authors at: Key Laboratory of Marine Materials and Related Technologies, Zhejiang Key Laboratory of Marine Materials and Protective Technologies, Ningbo Institute of Materials Technology and Engineering, Chinese Academy of Sciences, Ningbo 315201, China (H. Zhao).
E-mail addresses: zhaohaichao@nimte.ac.cn (H. Zhao), wangliping@nimte.ac.cn (L. Wang).

https://doi.org/10.1016/j.cej.2020.128301
Received 25 August 2020; Received in revised form 21 November 2020; Accepted 22 December 2020
Available online 28 December 2020

anticorrosion of waterborne epoxy (EP) coatings [21]. Compared with pure epoxy coatings, the as-prepared graphene/EP nanocomposite coatings have excellent barrier properties to corrosive media. Additionally, Mai and colleagues calculated the effect of nanosheets with different orientations on the barrier properties of the coating [22]. Studies have shown that in-plane parallel-oriented nano-sheets have a higher aspect ratio and can significantly enhance the barrier effect perpendicular to the orientation direction. Despite the excellent barrier properties of graphene-modified polymer coatings, graphene promotes corrosion of metals due to its high electrical conductivity [23-25]. This is because graphene is the cathode of most metals, leading to micro-electrical corrosion of the coating between graphene and metal interface at the defect, which will greatly hinder its application in long-term metal protection [13,25]. Zhou et al. confirmed that the corrosion enhancement of graphene is ascribed to its high intrinsic conductivity [26]. Schriver and co-workers also reported that battery circuits formed at the graphene-metal interface accelerated electrochemical corrosion of the metal [13]. Therefore, suppression of corrosion lies in inhibition of an electrochemical reaction path.

At present, the strategies to effectively address aforementioned issues and improve the anticorrosive performance of coatings mainly include encapsulation and development of new two-dimensional layered materials with low conductivity [27,28]. Sun et al. encapsulated graphene using a polymer ((3-aminopropyl)-triethoxysilane) through covalent interaction, significantly inhibiting its corrosion promoting activity [2]. This is because the (3-aminopropyl)-triethoxysilane molecule acts as a spacer to cut off the electron transfer path between graphene and the metal. However, it involves complex reaction processes and the graft rate of polymer chains in graphene is extremely low. In addition, reducing the conductivity of nanosheets through encapsulation has certain limitations, and to a large extent destroys the thin layer structure of graphene. Ding et al. found that transition metal dichalcogenides with low conductivity could not only increase the tortuous path of corrosion factor diffusion, but also effectively cut off the electron path of micro galvanic corrosion [29]. Ajayan et al. incorporated boron nitride (BN), which is hydrophobic, low in conductivity, and inert, into the polymer to improve the anti-corrosion performance of the coating [30]. However, such two-dimensional sheet material greatly increases the thickness of the additive and limits its utilization efficiency in the coating.

In this research, we designed a new anti-corrosion strategy inspired by natural nacre and mussels [31,32]. First, pre-deposited a layer of water-based epoxy resin on the surface of steel by electrophoretic deposition, then a nacre-mimic graphene oxide interlayers with controlled thickness was electrodeposited via mussel-inspired dopamine chemistry, and finally covered it with an epoxy resin by electrophoretic deposition to obtain a bionic epoxy-(graphene-dopamine)$_n$-epoxy sandwich anticorrosive coating. As a “binder”, DA contains a lot of amine groups and catechol, which is not only the anchor through which mussels are able to attach to surfaces, thereby improving the interface compatibility between epoxy resin and graphene, but also act as a coating itself to slow the substrate corrosion [33,34]. In addition, the hydrogen bonding between the ultra-thin GO nanosheets as a “brick” and DA, and the electrostatic interaction between $–COO^-$ in GO and $–NH_3^+$ in dopamine (pH = 6.7), so that graphene is parallel to the substrate and arranged between two epoxy coatings. Graphene arranged parallel to the substrate not only effectively impeding the penetration of corrosive medium, but also gives full play to the extraordinary impermeability of graphene. More importantly, the sandwich composite coating can shield galvanic corrosion by avoiding direct contact with the substrate. Finally, we control the number of graphene sheets to reveal the effect of natural nacre and mussel inspired graphene on the long-term corrosion properties of composite coatings.

2. Methods

2.1. Materials

Waterborne cathodic epoxy resin electrophoretic emulsion was provided by Jiangxi Gaojie Technology Co., Ltd. GO was purchased from Ashine Advanced Carbon Materials (Changzhou) Co., Ltd. Other reagents used in this study were purchased from Sigma-Aldrich Co., Ltd. (China) without further processing. Q235 mild steel was used as the substrate for composite coatings. Before use, it is polished with 600 and 1200C sandpaper, and then ultrasonically cleaned with acetone and ethanol for 20 min, respectively. A steel sheet with a size of 2 × 30 × 30 mm^3 (area of active electrode in electrolyte is 25 × 30 mm^2) is used for electrochemical coating.

2.2. Preparation of graphene oxide/dopamine electrolyte.

The 0.1 M phosphate buffer was prepared by adding an appropriate 0.1 M NaOH solution to the 0.1 M KH_2PO_4 solution until the pH reached 6.7. The buffer is stored in a dark environment at 4 °C. A solution containing dopamine hydrochloride with a concentration of 5 mM was prepared fresh before use, and then GO of the same mass as dopamine hydrochloride was added.

2.3. Cyclic voltammetry

The cyclic voltammetry was performed by a typical three-electrode electrochemical circuit on the Gamry electrochemical workstation. The steel pre-deposited with a layer of epoxy resin (area of active electrode in electrolyte is 25 × 30 mm^2) was used as the working electrode (WE), while the platinum mesh and Ag/AgCl (3 M KCl) electrodes were used as the counter electrode (CE) and the reference electrode (RE), respectively. Calibrate the reference electrode before use to ensure that the same reference potential is applied to each experiment. The scanning range is 0.1–1.1 V, and the scanning rate is set to 20 mV/s. Graphene arrangements with different layers are obtained by controlling the number of different cycles.

2.4. Characterization

The elemental composition of the samples and corrosion products of the steel surface were collected by XPS (Axis Ultra DLD, Kratos, UK) and Renishaw Invia spectrometer (Renishaw, UK). FEI Quanta FEG 250 (FEI) and S4800 (Hitachi) scanning electron microscopes were used to characterize the structure and morphology of coatings. The scanning probe microscope (SPM, Dimension 3100) was used to obtain the micromorphology and thickness of the sample. The microstructure of the sample was further obtained by using HRTEM (Talos F200x). The infrared spectra of rGO/PDA films with different layers are collected on the micro-infrared spectrometer (Cary660 + 620) with a wave number range of 500–4000 cm^{-1}. The XRD measurements of different samples were performed on D8 Advance Davinci (Brook AXS), where Cu-Kα radiation $\lambda = 1.54178$ Å, and the range is $10° \leq 2\theta \leq 90°$.

2.5. Corrosion behavior test of coatings.

The long-term corrosion resistance of different coatings was characterized by EIS testing and salt spray experiments. OCP and EIS tests for coatings under different immersion times were performed using a conventional three-electrode system at CHI-660E electrochemical workstation (Shanghai Chenhua, China). The coating, platinum sheet, and saturated calomel electrode are used as the WE (exposed area is 1 cm^2), CE, and RE of the three-electrode system, respectively. EIS test was conducted after the OCP was stable, in which the frequency range of EIS test was 10^5 to 10^{-2} Hz and the amplitude was set to 20 mV. The data recorded was fitted and analyzed using ZSimpWin software. After

immersion for 90 days, the coating on the steel surface was removed and the composition and distribution of corrosion products on the surface were evaluated by SEM (FEI Quanta FEG 250) and Renishaw Invia spectrometer (Renishaw, UK) to reveal the corrosion resistance mechanism. To prove the long-term anticorrosion of the coating in industrial applications, the coating was salt spray tested by spraying 5 wt% neutral NaCl solution. Before the salt spray test, artificial scratches were introduced to the coating surface with a scalpel.

3. Results and discussion

The schematic diagram of the bionic sandwich composite epoxy coating preparation process is shown in Fig. 1. The cleaned Q235 steel and Cu are used as the cathode and anode of electrophoretic deposition system, respectively. The electrophoretic emulsion of water-based cathode epoxy resin with 25% solid content was used as the electroplating solution, and a layer of epoxy resin was deposited on the surface of the steel using a direct-current (DC) power at ambient temperature. Then, graphene interlayer with controlled thickness was prepared by deposition of graphene oxide/dopamine electrolyte on the surface of the pre-deposited epoxy resin by cyclic voltammetry (CV). Finally, the upper epoxy layer coating was formed by electrodeposition and cured at 160 °C for 15 min to acquire the bionic sandwich composite epoxy coating. For simplicity, we denote the coatings prepared after 0, 1, 5, and 10 scanning cycles of graphene oxide dopamine electrolyte as pure-EP, L1-EP, L5-EP, L10-EP, respectively.

The graphene oxide/dopamine electrolyte consists of equal masses of GO and DA dispersed in 0.1 M phosphate buffer (pH = 6.7). Owing to the electrostatic interaction between $–COO^-$ in GO and $–NH_3^+$ in dopamine, the as-prepared GO/DA can be stably dispersed in a buffer solution of pH = 6.7 without precipitation (Fig. S1, Supporting Information). In addition, previous work has shown that there are significant differences in the formation mechanism of polydopamine (PDA) at different pH values because different dissociates will participate in the dopamine polymerization process [35]. To suppress the self-oxidation of dopamine in the solution and avoid side effects (e.g. steel corrosion and water electrolysis), we set the pH, scan rate, and scan range of GO/DA electrodeposition to 6.7, 20 mV/s, and 0.1–1.1 V, respectively. Fig. 2a1–a3 displays the cyclic voltammogram of repeated CV experiments in 0.1 M phosphate buffer (pH = 6.7). Apparently, the small oxidation peak appearing in the first cycle indicates that the reduced graphene oxide/polydopamine (rGO/PDA) was successfully deposited on the steel substrate of pre-deposited epoxy resin. However, the reduction peak is not obvious, indicating that the rGO/PDA deposited on the substrate is very dense. As the number of cycles increases, the decrease of the anode and cathode signals indicated the decrease of the GO/DA content in the solution and the deposition of the polydopamine insulating layer on the substrate, so there is almost no GO/DA deposition after 10 cycles [36]. Notably, due to the hydrogen bonding between GO nanosheets and DA, and the electrostatic interaction between $–COO^-$ in GO and $–NH_3^+$ in dopamine, graphene can be aligned parallel to the substrate under the action of an electric field.

The morphology and thickness of initial GO and modified GO/DA are characterized by TEM and SPM. It can be seen from Fig. 2b1, b2 that the original GO is complete, smooth, and transparent, and the average thickness of the single layer is about 0.83 nm, showing excellent dispersibility. The dopamine-modified GO still maintains a complete sheet structure and particles appear on the GO surface (Fig. 2b3), which is ascribed to the electrostatic interaction between $–COO^-$ in GO and $–NH_3^+$ in dopamine, resulting dopamine attached to the GO surface. The SPM results reveal that the average thickness of the modified GO/DA is about 4.49 nm (Fig. 2b4), indicating that the modified GO/DA still has a high aspect ratio.

In order to investigate the composition of rGO/PDA deposited on the surface of epoxy resin, we deposited different layers of rGO/PDA on steel sheets pre-deposited with an epoxy resin, and then directly cured at high temperature for Raman, XRD, infrared (IR), SPM, and XPS tests. Fig. 2c1–c3 collects the Raman and XPS spectra of rGO/PDA films for1, 5, and 10 scanning cycles (For convenience, record as L1-rGO/PDA, L5-rGO/PDA, and L10-rGO/PDA respectively.). It can be seen from the Raman spectra (Fig. 2c1) that the typical D and G peaks appear around 1340 and 1580 cm^{-1} [37]. Where, D peak represents the defect degree of carbon atom crystal. The fitting results show that the ratios of D peak to G peak (I_D/I_G) of L1-rGO/PDA, L5-rGO/PDA, and L10-rGO/PDA are 1.14, 1.07, and 1.04, respectively, indicating that increasing the number of graphene layers can effectively reduce the degree of defects in rGO/PDA films [38]. In addition, the increase in the number of graphene layers does not change the structure, which can be confirmed from the XRD spectrum (Fig. S2, Supporting Information). Specifically, graphene with different numbers of layers all have the (002) crystal plane of graphene around 26° (JCPDS 01–075-1621), and the intensity of the peak increases with the increase of the number of graphene layers.

The chemical bonding and composition of the samples can be analyzed from the XPS. In the C 1s fine spectrum (Fig. 2c2), after

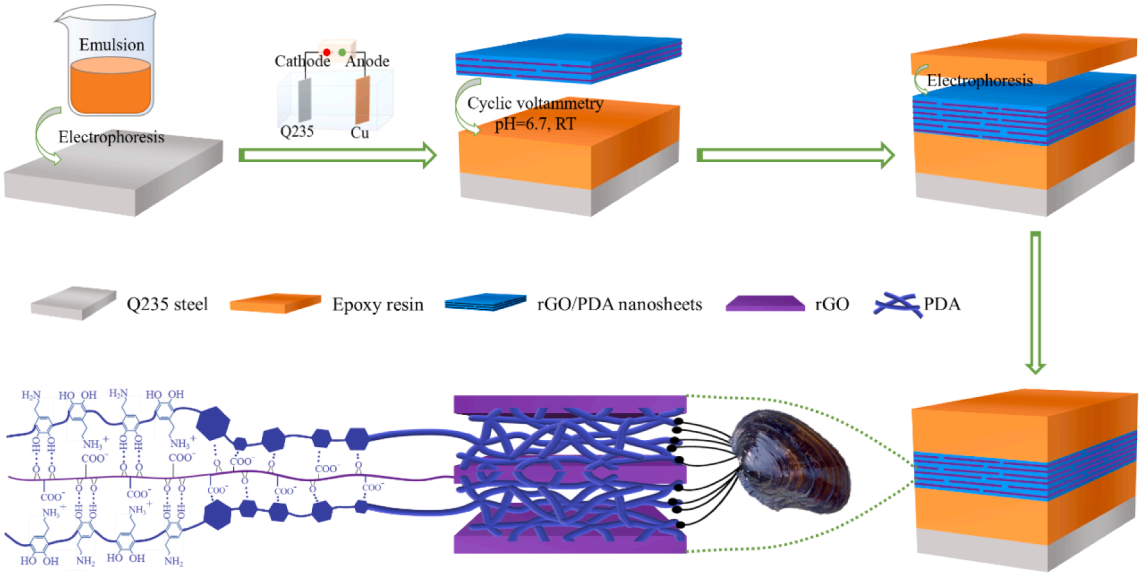

Fig. 1. Sketch of the preparation process of natural nacre and mussel inspired epoxy coating for sandwich.

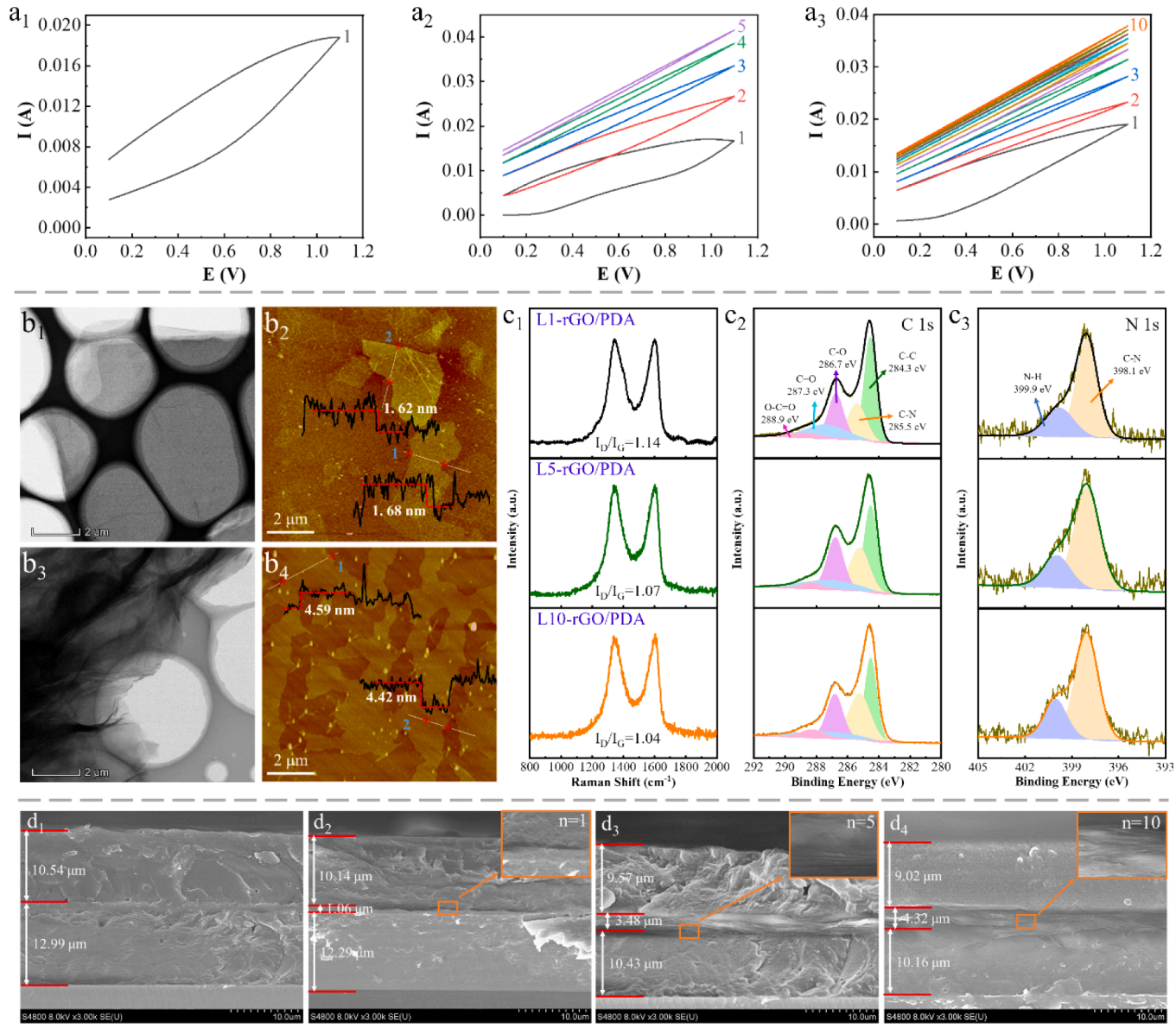

Fig. 2. a) Cyclic voltammograms at different cycles in 0.1 M phosphate buffer (pH = 6.7) of the a_1) 1 cycle, a_2) 5 cycles, and a_3) 10 cycles. b) TEM and SPM pictures of the b_1, b_2) GO and b_3, b_4) GO/DA dispersion in ethanol. c) rGO/PDA with different cycless of c_1) Raman spectra, c_2) XPS C 1s fine spectra, and c_3 XPS N 1s fine spectra. d) Cross-sectional SEM morphology of the d_1) pure-EP, d_2) L1-EP, d_3) L5-EP, and d_4) L10-EP coatings.

Gaussian fitting, L1-rGO/PDA, L5-rGO/PDA, and L10-rGO/PDA samples all contain five peaks of C–C, C–N, C–O, C═O, and O–C═O, which are located near 284.3, 285.5, 286.7, 287.3, and 288.9 eV, respectively [39]. Only the peak intensities are different, indicating that the structure of the three samples does not change much, which is consistent with the results of XRD and IR analysis (Figs. S2 and S3, Supporting Information). Similarly, the L1-rGO/PDA, L5-rGO/PDA, and L10-rGO/PDA samples all contained C-N (398.1 eV) and N–H (399.9 eV) peaks in the N 1 s fine spectrum (Fig. 2c3) [1]. Moreover, IR proves that the GO nanosheets and dopamine interact through hydrogen bonds (Fig. S3), and the strength of the hydrogen bonds increases with the number of cycles. The N − H stretching peak is slightly shifted from 1568.2 to 1563.7 cm^{-1}, and the C═O stretching peak is shifted from 1663.4 to 1658.8 cm^{-1}. Finally, we judged the denseness of the deposited rGO/PDA film through SPM test (50 × 50 μm), and the result is shown in Fig. S4 (Supporting Information). Obviously, the roughness of graphene films deposited with different numbers of layers increases with the increase of the number of graphene layers, and all exhibit good compactness. This is beneficial to enhance the barrier effect of the bionic sandwich coating and extend the diffusion path of corrosive media.

Fig. 2d1-d4 provides cross-sectional SEM morphology of pure-EP, L1-EP, L5-EP, and L10-EP coatings. The thickness of all coatings is maintained at approximately 23.5 μm via controlling electrodepositon conditions. Clearly, the water-based epoxy coating deposited on the surface of the steel sheet by electrophoresis is very dense. Fig. 2d1 is a cross-sectional SEM image of a pure epoxy coating without deposition of rGO/PDA, in which two layers of obvious epoxy resin appear, and the thickness of the upper layer of epoxy resin is lower than that of the lower layer of epoxy resin, which is caused by the decreased conductivity of the substrate after the deposition of one layer of epoxy resin. For the L1-EP coating (Fig. 2d2), there is a clear layer of rGO/PDA between the two epoxy resin layers, which is about 1.06 μm and is arranged parallel to the substrate. It is important that as the number of CV experiment cycles increases, the number of rGO/PDA layers in the coating also increases, and they are all arranged parallel to the substrate. However, due to the reduced GO/DA content in the solution and the insulation properties of the polydopamine, the thickness of the subsequently deposited rGO/PDA decreased. The arrangement of rGO/PDA parallel to the substrate is

ascribed to the electrostatic interaction between $–COO^-$ in GO and $–NH_3^+$ in dopamine. Under the action of an electric field, dopamine deposits and adheres to the surface of the epoxy resin. The $–NH_3^+$ on the surface of the dopamine will cause electrostatic interaction with $–COO^-$ in GO, so that the graphene is arranged parallel to the substrate. This kind of graphene arranged parallel to the substrate can fully exert the interaction between its high surface area and electrolyte, and has better physical barrier effect. Furthermore, the graphene arranged parallel to the substrate can more effectively prevent the penetration of the corrosion medium, and significantly extend the diffusion path of the corrosion medium, so that the composite coating has superior corrosion resistance.

To investigate the influence of graphene incorporation on the corrosion resistance of coatings, the long-term anti-corrosion behavior of different coatings is compared by EIS and salt spray tests. The coatings are immersed in homemade simulated salt water (3.5 wt% NaCl, pH = 7), and EIS tests were performed on coatings with immersion times of 1, 10, 30, 60, and 90 days. Before the coating is subjected to the EIS test, open circuit potential (OCP) testing is performed on the coating to stabilize it in the corrosion solution. The change of the OCP value of the sample with the immersion time is shown in Fig. S5 (Supporting Information). As the immersion time increases, the OCP of pure-EP and L1-EP coatings becomes negative. The corrosive medium penetrates and reaches the substrate at 30 and 60 days respectively, causing the coating failure. Compared with pure-EP coating, L1-EP coating reduces the penetration rate owing to the presence of single-layer graphene. However, due to the presence of mussel inspired graphene in L5-EP and L10-EP coatings, the impermeability of the coatings is significantly improved, and the OCP value is still as high as −0.12 and 0.046 after 90 days of immersion, respectively.

The Bode and Bode-Phase curves of pure-EP, L1-EP, L5-EP, and L10-EP coatings are listed in Fig. 3a, b. Generally, the higher the impedance of the coating at $f = 0.01$ Hz ($|Z|_{0.01Hz}$), the better the corrosion protection effect [40]. In addition, when corrosive substances reach the substrate and cause metal corrosion, two time constants are generated in the Bode-Phase diagram [11]. It can be seen from the Bode diagram (Fig. 3a1–a4) that on the first day of immersion, as the number of graphene scans increases, the resistance value of the coating at low frequencies becomes larger and larger. When the number of graphene scans is 10, the $|Z|_{0.01Hz}$ of the L10-EP coating is 5.25×10^{10} O cm^2, one order of magnitude higher than that of pure coating (4.11×10^9 O cm^2). It indicates that incorporating the bionic graphene sheet can significantly enhance the anticorrosion performance of the coating. With the increase of the immersion time, the $|Z|_{0.01Hz}$ of the pure-EP coating decreases sharply, and the corrosion rate reached its maximum when the immersion time is 30 days. This can also be seen from the Bode-Phase curve (Fig. 3b1). When the pure-EP coating is immersed for 30 days, two phase angle constants appear, showing that the corrosion medium reaches the substrate and the coating fails. After immersion for 90 days, the $|Z|_{0.01Hz}$ of the pure-EP coating decreased to 6.46×10^6 O cm^2, which displayed poor permeability resistance.

The $|Z|_{0.01Hz}$ of L1-EP coating after immersion for one day is 9.12×10^9 O cm^2. After 90 days, the $|Z|_{0.01Hz}$ decreased to 6.17×10^7 O cm^2. It can be seen from the Bode-Phase curve (Fig. 3b2) that the L1-EP coating has two phase angle constants when it is immersed for 60 days, which indicates that the L1-EP coating has failed at 60 days. Compared to the pure-EP coating, the impedance modulus value of the doped graphene coating increases, and the corrosion rate becomes slower. This shows that the incorporation of graphene arranged parallel to the substrate into the coating can significantly enhance the barrier effect of the biomimetic sandwich coating, thereby slowing down the penetration of corrosive substances and enhancing the anticorrosion of the coating. In terms of L5-EP coating, the initial $|Z|_{0.01Hz}$ is 3.63×10^{10} O cm^2. After 90 days, the $|Z|_{0.01Hz}$ remains at 5.13×10^8 O cm^2, and the Bode-Phase curve

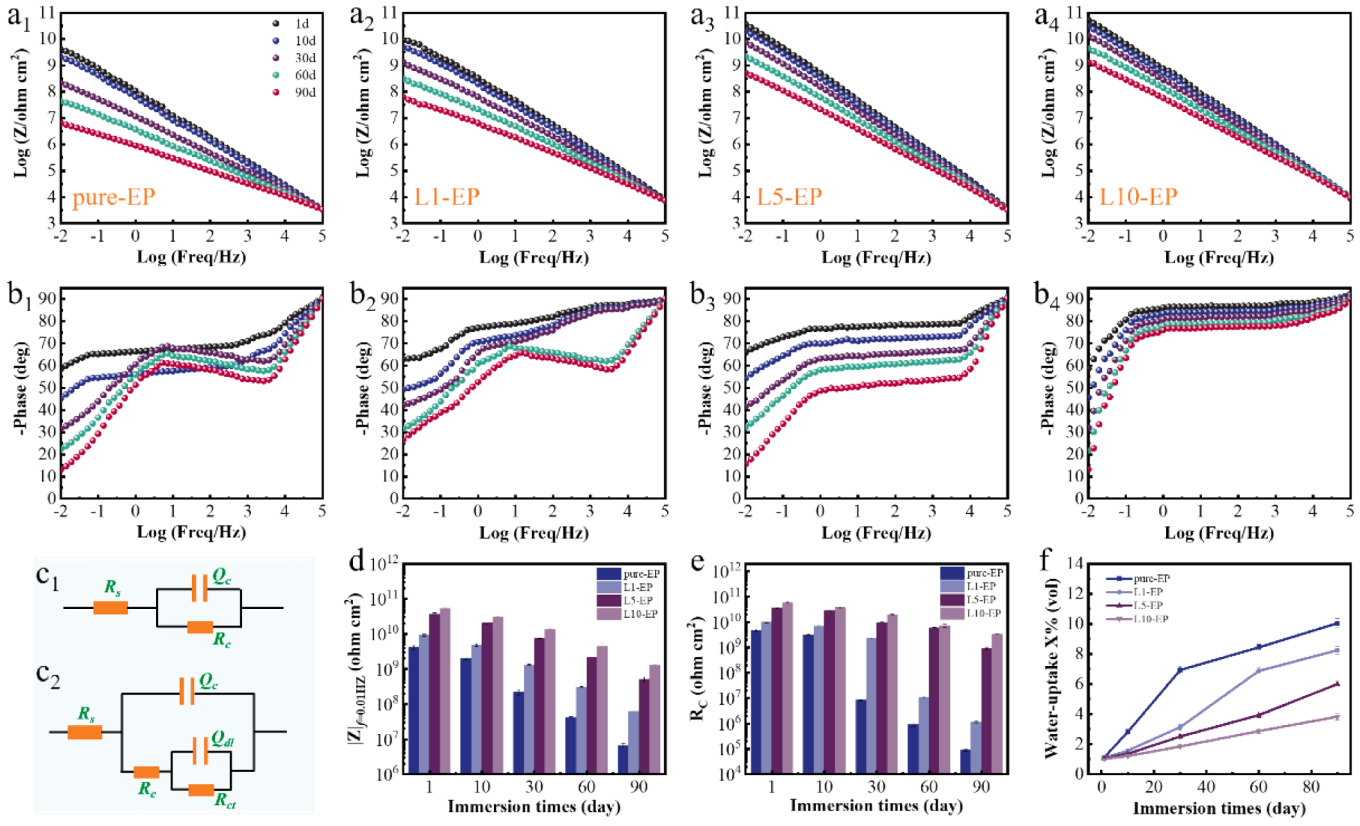

Fig. 3. a, b) Bode and Bode-Phase plots of the a_1, b_1) pure-EP, a_2, b_2) L1-EP, a_3, b_3) L5-EP, and a_4, b_4) L10-EP coatings in simulated seawater. c) Simulation circuit diagram of the bionic sandwich coating at different stages. d) $|Z|_{0.01Hz}$, e) R_c, and f) water absorption of coatings.

(Fig. 3b3) only displays one phase angle constant, indicating that the corrosive substance has not yet reached the surface of the steel substrate. It shows that the increase in the number of graphene layers is beneficial to further improve the corrosion resistance of the biomimetic sandwich coating and reduce the corrosion rate. This is due to the increase in the number of graphene layers can fill the defects in single-layer graphene, which is more conducive to the use of graphene's impermeability. Surprisingly, after being immersed for 90 days, the $|Z|_{0.01Hz}$ of the L10-EP coating is still up to 1.32×10^9 O cm^2, showing extraordinary corrosion resistance. Moreover, it can be seen from the Bode-Phase curve (Fig. 3b4) that the phase angle of the L10-EP coating has been kept below $-80°$ in the high frequency region, indicating that the corrosive substances is far from the substrate. The improvement of the anticorrosion of the composite coating is attributed to the graphene arranged parallel to the substrate, which effectively prevents the penetration and prolongs the diffusion path of corrosive media, and give full use of the extraordinary impermeability of graphene. More importantly, the bionic sandwich composite coating can shield galvanic corrosion by avoiding direct contact with the substrate.

The Nyquist diagrams of pure-EP, L1-EP, L5-EP, and L10-EP coatings under different immersion times are listed in Fig. S6 (Supporting Information). It can also be seen that the pure-EP coating (Fig. S6a-ii) and L1-EP coating (illustration in Fig. S6b) have two time constants after 30 and 60 days, respectively, indicating that the corrosive medium has reached the substrate [41,42]. Generally speaking, the analog circuit can be divided into two stages according to whether the corrosive substance reaches the substrate. When corrosive substances reach the surface of the steel substrate, as shown in Fig. 3c2, otherwise it is shown in Fig. 3c1 [43]. In the equivalent circuit model diagram, R_s represents solution resistance, R_c and R_{ct} represent the resistance and charge transfer resistance of the coating, respectively, and Q_c and Q_{dl} are the capacitance and double layer capacitance of the coating, respectively [44]. In general, the impedance arc radius in the Nyquist diagram reflects the corrosion resistance of the coating. Previous studies have shown that the larger the arc radius of the impedance, the better the coating's corrosion resistance [45]. The $|Z|_{0.01Hz}$ and R_c values obtained through fitting are shown in Fig. 3d, e. Obviously, the anti-corrosion performance of the coating decreases as the immersion time increases. Pure coating and L1-EP coating have the fastest rate of decrease in R_c at 30 and 60 days, respectively, which also proves that corrosive substances penetrate to the substrate. However, the corrosion reduction rate of L10-EP coating is the slowest, and the R_c is still up to 1.30×10^9 O after 90 days, which indicates that the addition of graphene can significantly reduce the penetration rate of corrosive media. This is due to the fact that the multi-layer graphene can fill the defects in the single-layer graphene, which is more conducive to exerting the impermeability of graphene and enhancing the physical barrier effect of the coating. Therefore, the coating shows satisfactory anti-corrosion performance.

To study and compare the influence of different number of graphene sheets on the impermeability of the coating, we calculated the water absorption of the bionic sandwich coating by Brasher-Kingsbury formula (Eq. (1)) [46-48]. The calculated result is shown in Fig. 3f.

$$X_v\% = \frac{log\frac{C_c\ (t)}{C_c\ (0)}}{log(80)} \times 100 \quad (1)$$

In the formula, X_v (%) is the volume fraction of water in the coating, and C_c (0) and C_c (t) are the dry film capacitance and instantaneous capacitance respectively. Clearly, the change law of the water absorption of the bionic sandwich coating is opposite to the change law of the corrosion resistance. The results show that graphene arranged in parallel can significantly improve the coating's resistance to water penetration. Furthermore, the water absorption of pure-EP and L1-EP coatings increased sharply at 30 and 60 days, respectively. This corresponds to the failure time of the coating, indicating that the failure of the coating is caused by the penetration of corrosive media into the substrate. Notably, as the number of graphene scans increases, the barrier properties of the coatings increase significantly. Especially L10-EP coating, even after soaking for 90 days, the water absorption rate is only 3.82%, showing outstanding physical barrier effect.

To demonstrate the long-term anticorrosion of the bionic sandwich coating in industrial applications, salt spray tests are performed by spraying a 5 wt% neutral NaCl solution. Artificial scratches are introduced into the coating surface with a scalpel prior to salt spray testing. Fig. 4a provides optical images of pure-EP, L1-EP, L5-EP, and L10-EP coatings tested at 0, 120, 240 and 480 h. The pure-EP coating (Fig. 4a1) is tested for 120 h, the area around the scratch is almost completely covered by rust. After 240 h of testing, the corrosion around the scratch further spread outward, and corrosion spots appeared on the coating surface, showing that the corrosive medium has reached the substrate, causing steel corrosion. After the 480 h test, the coating corrosion became more and more serious, and bubbles appeared on the surface of the coating, indicating that the coating began to fall off, with little protective effect. For the L1-EP coating (Fig. 4a2), only a few rust spots appeared around the scratches at 120 h. After 240 h of testing, only the corrosion around the scratch became serious, and the coating surface remained intact. However, after 480 h, corrosion spots began to appear on the coating surface, demonstrating the penetration of the corrosive medium. Comparing L1-EP coating and pure-EP coating, it is found that the incorporation of graphene can significantly intensify the impermeability and corrosion resistance of the coating. In particular, after the L5-EP and L10-EP coatings (Fig. 4a3, a4) are subjected to a salt spray test for 480 h, the coating surfaces remained intact. Moreover, the corrosion rate of L10-EP coating is slower than that of L5-EP coating, which is consistent with the conclusion obtained by EIS test. This is because multilayer graphene sheets can fill defects in single graphene sheet, which is more conducive to exerting the impermeability of graphene and enhancing the barrier effect of the bionic sandwich coating. In addition, natural nacre and mussel inspired graphene can further extend the diffusion path of corrosive substances, and the coating exhibits unexpected anticorrosive properties.

To compare the influence of different numbers of graphene sheets on the biomimetic sandwich coating. We used SEM, XPS and Raman tests to analyze the corrosion products of the coating substrate surface after 90 days of immersion in simulated seawater. Before analysis of corrosion products, the coating on the substrate surface was removed and washed with ethanol. The SEM images and corresponding element distributions of the corrosion products on the carbon steel surface of pure-EP, L1-EP, L5-EP, and L10-EP coatings are shown in Fig. 4b. The surface of carbon steel under pure coating is severely corroded and almost completely covered by corrosion products (Fig. 4b1). The surface is mainly composed of Fe, O and a few Cl elements, manifesting that the corrosive material passes through the defects of the coating surface and triggers the oxidation reaction of the substrate surface. For the L1-EP coating (Fig. 4b2), most of the surface of the carbon steel is also covered by corrosion products. The main elements are still Fe, O, and a little Cl, which is related to its poor protective performance. However, compared to pure-EP coatings, corrosion products are reduced. Some corrosion products appeared on the surface of the carbon steel under L5-EP coating (Fig. 4b3), mainly composed of Fe and a few O elements. This may be that after 90 days of immersion, the corrosive medium just reached the substrate, but it has not caused the coating failure. Nonetheless, the carbon steel surface of the L10-EP coating has almost no corrosion products (Fig. 4b4), and is mainly composed of Fe elements. Exhibits extraordinary impermeability and outstanding corrosion resistance.

To further determine the composition of corrosion products on the steel surface, XPS and Raman tests are performed on the samples, as shown in Fig. 5a. For pure-EP and L1-EP coatings, after Gaussian fitting, the Fe element in the corrosion products can be fitted to five peaks, including Fe (707.0 eV), Fe $2P_{3/2}$ in Fe_2O_3/Fe_3O_4 (708.6 eV), Fe $2P_{3/2}$ in Fe (III) (e.g., FeO or $FeCl_2$) (715.6 eV), Fe $2P_{1/2}$ in Fe_2O_3/Fe_3O_4 (721.4 eV), and Fe $2P_{1/2}$ in Fe (III) (729.3 eV). This is because pure-EP and L1-

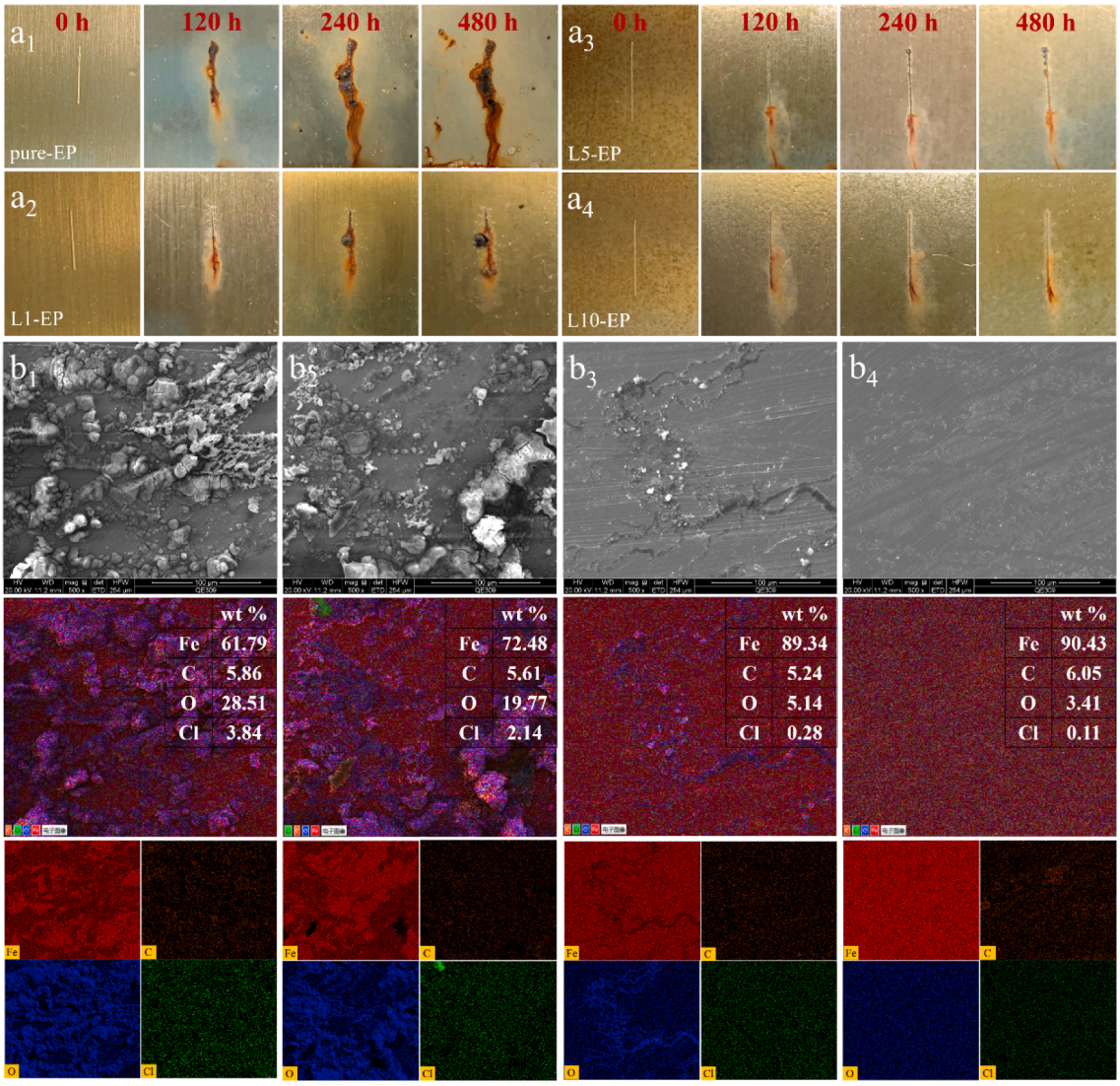

Fig. 4. a) The optical images of the a_1) pure-EP, a_2) L1-EP, a_3) L5-EP, and a_4) L10-EP coatings tested at 0, 120, 240, and 480 h. b) SEM image of steel surface and corresponding element distribution after 90 days immersion of the b_1) pure-EP, b_2) L1-EP, b_3) L5-EP, and b_4) L10-EP coatings.

EP coatings have poor permeability to the corrosive medium, reaching the substrate at 30 and 60 days, respectively, resulting in coating failure. Therefore, after 90 days of immersion, there are a lot of corrosion products on the surface of the carbon steel, and it is mainly composed of $FeCl_2$ and Fe_2O_3/Fe_3O_4. However, after 90 days of immersion in the L5-EP coating, the corrosive medium (especially H_2O) just reached the substrate but did not cause the coating to fail. Therefore, the carbon steel surface is mainly composed of Fe_2O_3/Fe_3O_4 and a small amount of $FeCl_2$ [49,50]. For the L10-EP coating, the corrosive substances are still far away from the substrate due to the excellent barrier properties and "maze effect" of parallel arrangement of graphene, so only Fe_2O_3/Fe_3O_4 signal peak is detected on the surface of carbon steel. This is probably caused by the oxidation of exposed steel in the air.

Fig. 5b shows the Raman test results of corrosion products on the steel surface. The peak position of the corrosion products of the pure-EP coating is very obvious, indicating that the content of corrosion products is large, and is mainly composed of γ-FeOOH (215.8 and 1289.3 cm^{-1}) [51], α-FeOOH (282.8 cm^{-1}) [52], β-FeOOH (395.1 and 600.1 cm^{-1}) [50,53], and Fe_3O_4 (671.7 cm^{-1}) [54,55] composition. The corrosion products of L1-EP coating are almost the same as those of pure-EP coating, except that the characteristic peak intensity is reduced, showing that the content of corrosion products is reduced. For the L5-EP coatings, characteristic peaks are observed around 215.8, 282.8, 395.1, and 719.3 cm^{-1}, which correspond to γ-FeOOH, α-FeOOH, β-FeOOH, and Fe_3O_4, respectively, and the characteristic peak intensity is reduced. However, only characteristic peak of Fe_3O_4 is found at 719.3 cm^{-1} in the L10-EP coating, which indicates that the corrosive solution has not reached the substrate, exhibits extraordinary resistance to water penetration. In general, the anions in β-FeOOH body-centered cubic meters are arranged at a relatively low density, which is easy for electrochemical reduction and accelerates metal corrosion in environments containing chloride ions [56]. It is worth mentioning that compared with other similarly published works, the *L*10-EP coating shows better corrosion resistance under different immersion times (Fig. 5c) [1,11,17,21,42,57-60].

The anti-corrosion mechanism sketches of pure-EP, L1-EP, L5-EP and L10-EP coatings are shown in Fig. 6. The coating will prevent the corrosive substances from penetrating into the surface of substrate according to its resistance to permeability during the long immersion process of the corrosive solution (e.g·H_2O, O_2, and Cl^-). The corrosion process of the coating is an electrochemical reaction involving both anode and cathode reactions. As the immersion time continues, more corrosive media pass through the coating and reach the substrate to undergo the following electrochemical reactions (Eqs. (2)–(7)).

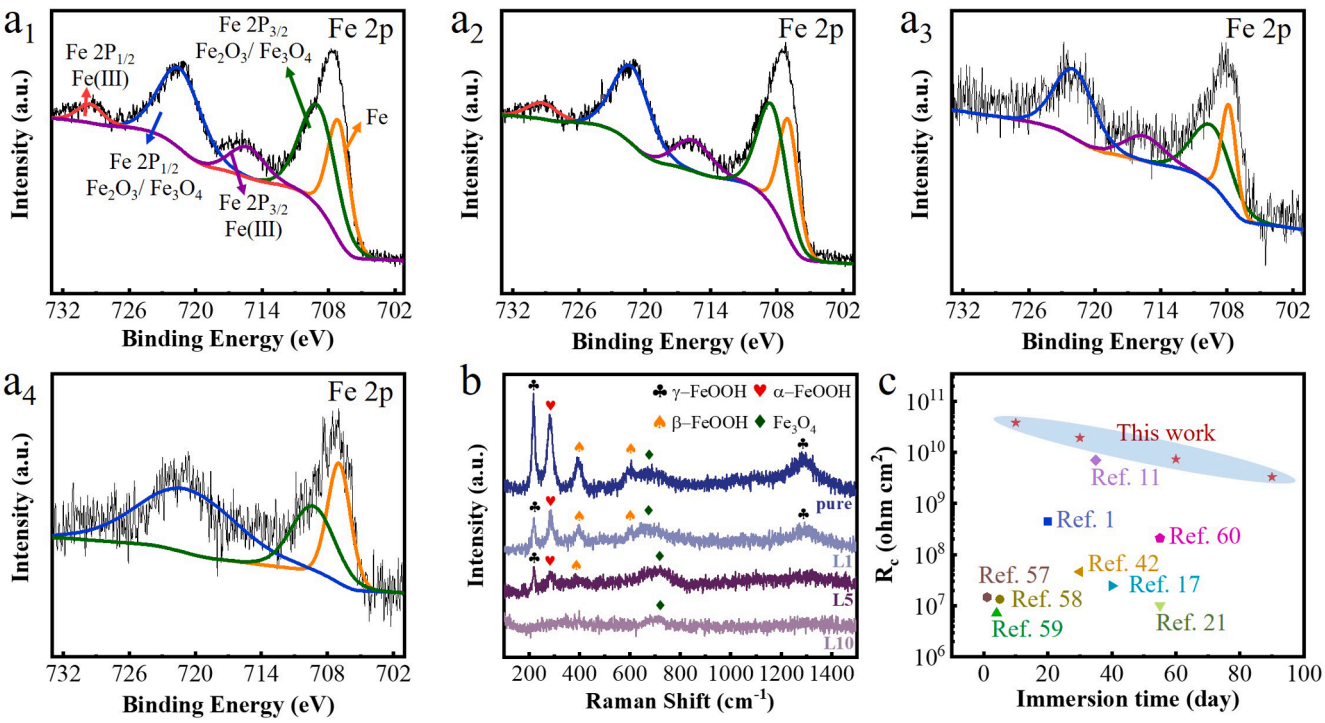

Fig. 5. a) XPS-Fe 2p spectrum of the a_1) pure-EP, a_2) L1-EP, a_3) L5-EP, and a_4) L10-EP. b) Raman spectrum of steel surface after coatings immersion for 90 days. c) Comparison of R_c between our L10-EP coating and previously reported graphene-modified coatings at different immersion times.

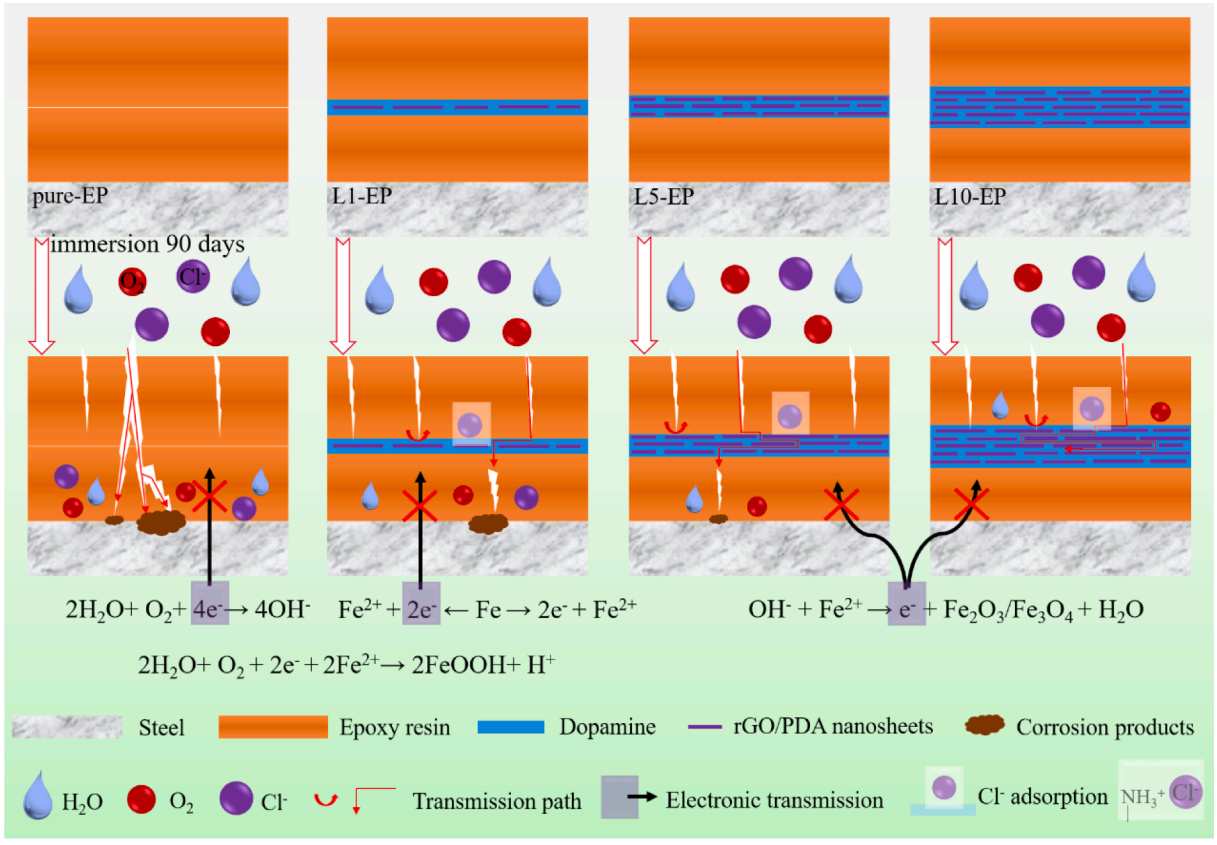

Fig. 6. Schematic diagram of coatings anticorrosion mechanism in our strategy.

$$Fe \rightarrow Fe^{2+} + 2e^{-} \quad (2)$$

$$Fe^{2+} \rightarrow Fe^{3+} + e^{-} \quad (3)$$

$$H_2O + \frac{1}{2}O_2 + 2e^- \rightarrow 2OH^- \quad (4)$$

$$2Fe^{2+} + 6OH^- \rightarrow Fe_2O_3 + 3H_2O + 2e^- \quad (5)$$

$$3Fe^{3+} + 8OH^- + e^- \rightarrow Fe_3O_4 + 4H_2O \quad (6)$$

$$2Fe^{2+} + 2H_2O + O_2 + 2e^- \rightarrow 2FeOOH + 2H^+ \quad (7)$$

For the pure-EP coating, due to the poor barrier property of the water-based epoxy resin itself, after 30 days of immersion, the corrosive medium reached the surface of the substrate. An electrochemical reaction occurs on the steel surface to form pitting pits, which further accelerates corrosion and invalidates the coating. Due to the presence of more corrosive media (H_2O, O_2), the surface of carbon steel is mainly composed of FeOOH or $FeCl_2$ and Fe_2O_3/Fe_3O_4. However, owing to the addition of rGO/PDA in the composite coating, the permeability of the coating is improved and it shows good anticorrosion. In the case of L1-EP coatings, the addition of single-layer rGO/PDA prevents part of corrosive media penetration and prolongs the diffusion path of the corrosive media. In addition, the $-NH_3^+$ on the PDA can adsorb Cl^- in the corrosion solution and slow down the coating corrosion. But because there are many defects in the single-layer rGO/PDA, the coating fails after 60 days of immersion. Similarly, there are more corrosive media on the surface of carbon steel after 90 days of immersion, so the surface of carbon steel is also mainly composed of FeOOH or $FeCl_2$ and Fe_2O_3/Fe_3O_4. For L5-EP coating, multilayer graphene sheets can fill defects in single graphene sheet, which is more conducive to exerting the impermeability of graphene and enhancing the barrier effect of the bionic coating. Therefore, the coating has not failed after 90 days of immersion, and shows excellent corrosion resistance. Surprisingly, the L10-EP coating exhibits satisfactory corrosion resistance, which can be attributed to three reasons. Firstly, the graphene arranged parallel to the substrate not only gives full play to the interaction between its high surface area and electrolyte to achieve the barrier limit of graphene, but also effectively prevents the penetration of the corrosive medium and prolongs the diffusion path of the corrosive substances. Secondly, the bionic sandwich composite coating can shield galvanic corrosion by avoiding direct contact with the substrate. Finally, the presence of dopamine enhances the interfacial compatibility between graphene and epoxy matrix, and gives graphene bionic nacre structure to achieve long-term protection of the substrate.

4. Conclusions

In this work, inspired by nature mussels and nacre, a sandwich-like anticorrosive epoxy coating containing dopamine functionalized graphene interlayers was successfully by electrodeposition methods. The presence of dopamine enhances the interfacial adhesion and compatibility between graphene and epoxy matrix, and gives graphene bionic nacre structure to achieve long-term protection of the substrate. Due to the electrostatic interaction between $-COO^-$ in graphene oxide and $-NH_3^+$ in dopamine (pH = 6.7) and the hydrogen bonding between GO and DA, graphene interlayers are parallel to the substrate and arranged between two epoxy coatings. The graphene sheets arranged parallel to the substrate effectively prevents the penetration and prolongs the diffusion path of corrosive media, and give full use of the extraordinary impermeability of graphene. More importantly, the bionic sandwich composite coating avoids the direct contact between graphene and the substrate, thereby shielding the galvanic corrosion. The results show that the composite coating prepared by 10 scanning cycle's graphene interlayers exhibits the most superior anticorrosion. Therefore, this study highlights a potential strategy to prepare biomimetic coatings with outstanding long-term anticorrosion.

Declaration of Competing Interest

The authors declare that they have no known competing financial interests or personal relationships that could have appeared to influence the work reported in this paper.

Acknowledgements

The study was supported by the National Science Fund for Distinguished Young Scholars of China (No.51825505), K.C.Wong Education Foundation (GJTD-2019-13), Zhejiang Key Research and Development Program (2019C03093), Strategic Priority Research Program of the Chinese Academy of Sciences (No.XDA13040601) and "One Hundred Talented People" of the Chinese Academy of Sciences (No. Y60707WR04).

Appendix A. Supplementary data

Supplementary data to this article can be found online at https://doi.org/10.1016/j.cej.2020.128301.

References

[1] X.H. Luo, J.W. Zhong, Q.L. Zhou, S. Du, S. Yuan, Y.L. Liu, Cationic reduced graphene oxide as self-aligned nanofiller in the epoxy nanocomposited coating with excellent anticorrosive performance and its high antibacterial activity, ACS Appl. Mater. Interfaces 10 (2018) 18400–18415.
[2] W. Sun, L. Wang, T. Wu, M. Wang, Z. Yang, Y. Pan, G. Liu, Inhibiting the corrosion-promotion activity of graphene, Chem. Mater. 27 (7) (2015) 2367–2373, https://doi.org/10.1021/cm5043099.
[3] M. Mao, L.i. Jiang, L. Wu, M. Zhang, T. Wang, The structure control of ZnS/graphene composites and their excellent properties for lithium-ion batteries, J. Mater. Chem. A 3 (25) (2015) 13384–13389, https://doi.org/10.1039/C5TA01501D.
[4] H. Bai, Y. Xu, L.u. Zhao, C. Li, G. Shi, Non-covalent functionalization of graphene sheets by sulfonated polyaniline, Chem. Commun. (13) (2009) 1667, https://doi.org/10.1039/b821805f.
[5] O.C. Compton, S. Kim, C. Pierre, J.M. Torkelson, S.T. Nguyen, Crumpled graphene nanosheets as highly effective barrier property enhancers, Adv. Mater. 22 (42) (2010) 4759–4763, https://doi.org/10.1002/adma.201000960.
[6] R.R. Nair, H.A. Wu, P.N. Jayaram, I.V. Grigorieva, A.K. Geim, Unimpeded permeation of water through helium-leak-tight graphene-based membranes, Science 335 (6067) (2012) 442–444, https://doi.org/10.1126/science:1211694.
[7] S.M. Ren, M.J. Cui, W.S. Li, J.B. Pu, Q.J. Xue, L.P. Wangs, N-doping of graphene: toward long- term corrosion protection of Cu, J. Mater. Chem. A 6 (2018) 24136–24148.
[8] K.S. Novoselov, V.I. Fal'ko, L. Colombo, P.R. Gellert, M.G. Schwab, K. Kim, A roadmap for graphene, Nature 490 (7419) (2012) 192–200, https://doi.org/10.1038/nature11458.
[9] N.T. Kirkland, T. Schiller, N. Medhekar, N. Birbilis, Exploring graphene as a corrosion protection barrier, Corros. Sci. 56 (2012) 1–4, https://doi.org/10.1016/j.corsci.2011.12.003.
[10] G. Cui, Z.X. Bi, R.Y. Zhang, J.G. Liu, X. Yu, Z.L. Li, A comprehensive review on graphene-based anti-corrosive coatings, Chem. Eng. J. 373 (2019) 104–121, https://doi.org/10.1016/j.cej.2019.05.034.
[11] X.B. Zhu, Q.Q. Yan, L. Cheng, H. Wu, H.C. Zhao, L.P. Wang, Self-alignment of cationic graphene oxide nanosheets for anticorrosive reinforcement of epoxy coatings, Chem. Eng. J. 389 (2020), 124435.
[12] D. Prasai, J.C. Tuberquia, R.R. Harl, G.K. Jennings, K.I. Bolotin, Graphene: corrosion-inhibiting coating, Acs Nano 6 (2012) 1102–1108.
[13] M. Schriver, W. Regan, W.J. Gannett, A.M. Zaniewski, M.F. Crommie, A. Zettl, Graphene as a long-term metal oxidation barrier: worse than nothing, ACS Nano 7 (7) (2013) 5763–5768, https://doi.org/10.1021/nn4014356.
[14] R. Singh Raman, A. Tiwari, Graphene: the thinnest known coating for corrosion protection, JOM 66 (2014) 637–642.
[15] R.K. Singh Raman, A. Tiwari, Long-term corrosion protection of a cupro-nickel alloy due to graphene coating, Coatings 7 (2017) 210.
[16] R. Singh Raman, A. Tiwari, Durable corrosion resistance of copper due to multi-layer graphene, Materials 10 (2017) 1112.
[17] M.J. Cui, S.M. Ren, H.C. Zhao, Q.J. Xue, L.P. Wang, Polydopamine coated graphene oxide for anticorrosive reinforcement of water-borne epoxy coating, Chem. Eng. J. 335 (2018) 255–266, https://doi.org/10.1016/j.cej.2017.10.172.
[18] Fandi Meng, Li Liu, Wenliang Tian, Hang Wu, Ying Li, Tao Zhang, Fuhui Wang, The influence of the chemically bonded interface between fillers and binder on the failure behaviour of an epoxy coating under marine alternating hydrostatic pressure, Corros. Sci. 101 (2015) 139–154, https://doi.org/10.1016/j.corsci.2015.09.011.

[19] M.J. Cui, S.M. Ren, J.B. Pu, Y.G. Wang, H.H. Zhao, L.P. Wan, Poly(o-phenylenediamine) modified graphene toward the reinforcement in corrosion protection of epoxy coatings, Corros. Sci. 159 (2019), 108131.

[20] C.H. Chang, T.C. Huang, C.W. Peng, T.C. Yeh, H.I. Lu, W.I. Hung, C.J. Weng, T. I. Yang, J.M. Yeh, Novel anticorrosion coatings prepared from polyaniline/graphene composites, Carbon 50 (14) (2012) 5044–5051, https://doi.org/10.1016/j.carbon.2012.06.043.

[21] S.H. Qiu, W. Li, W.R. Zheng, H.C. Zhao, L.P. Wang, Synergistic effect of polypyrrole-intercalated graphene for enhanced corrosion protection of aqueous coating in 3.5% NaCl solution, ACS Appl. Mater. Interfaces 9 (39) (2017) 34294–34304, https://doi.org/10.1021/acsami.7b08325.s001.

[22] C.S. Lu, Y.W. Mai, Influence of aspect ratio on barrier properties of polymer-clay nanocomposites, Phys. Rev. Lett. 95 (2005), 088303.

[23] L.J. Cao, X.Q. Liu, H.N. Na, Y.G. Wu, W.G. Zheng, J. Zhu, How a bio-based epoxy monomer enhanced the properties of diglycidyl ether of bisphenol A (DGEBA)/graphene composites, J. Mater. Chem. A 1 (16) (2013) 5081, https://doi.org/10.1039/c3ta01700a.

[24] L.T. Shen, Y.D. Zhao, Y. Wang, R.B. Song, Q. Yao, S.S. Chen, Y. Chai, A long-term corrosion barrier with an insulating boron nitride monolayer, J. Mater. Chem. A 4 (14) (2016) 5044–5050, https://doi.org/10.1039/C6TA01604A.

[25] C.L. Cui, A.T.O. Lim, J.X. Huang, A cautionary note on graphene anti-corrosion coatings, Nature Nanotech 12 (9) (2017) 834–835, https://doi.org/10.1038/nnano.2017.187.

[26] F. Zhou, Z.T. Li, G.J. Shenoy, L. Li, H.T. Liu, Enhanced room-temperature corrosion of copper in the presence of graphene, ACS Nano 7 (8) (2013) 6939–6947, https://doi.org/10.1021/nn402150t.

[27] Ji-Heng Ding, Hong-Ran Zhao, Yan Zheng, Xinpeng Zhao, Hai-Bin Yu, A long-term anticorrsive coating through graphene passivation, Carbon 138 (2018) 197–206, https://doi.org/10.1016/j.carbon.2018.06.018.

[28] Wen Sun, Lida Wang, Tingting Wu, Yanqiu Pan, Guichang Liu, Inhibited corrosion-promotion activity of graphene encapsulated in nanosized silicon oxide, J. Mater. Chem. A 3 (32) (2015) 16843–16848, https://doi.org/10.1039/C5TA04236D.

[29] Jiheng Ding, Hongran Zhao, Xinpeng Zhao, Beiyu Xu, Haibin Yu, How semiconductor transition metal dichalcogenides replaced graphene for enhancing anticorrosion, J. Mater. Chem. A 7 (22) (2019) 13511–13521, https://doi.org/10.1039/C9TA04033A.

[30] Esam Husain, Tharangattu N. Narayanan, Jose Jaime Taha-Tijerina, Soumya Vinod, Robert Vajtai, Pulickel M. Ajayan, Marine corrosion protective coatings of hexagonal boron nitride thin films on stainless steel, ACS Appl. Mater. Interfaces 5 (10) (2013) 4129–4135, https://doi.org/10.1021/am400016y.

[31] C.Q. Zhao, P.C. Zhang, J.J. Zhou, S.H. Qi, Y. Yamauchi, R.R. Shi, R.C. Fang, Y. Ishida, S.T. Wang, A.P. Tomsia, L. Jiang, M.J. Liu, Layered nanocomposites by shear-flow-induced alignment of nanosheets, Nature 580 (7802) (2020) 210–215, https://doi.org/10.1038/s41586-020-2161-8.

[32] Yuanyuan Zhang, Jingsong Peng, Mingzhu Li, Eduardo Saiz, Stephan E. Wolf, Qunfeng Cheng, Bioinspired Supertough Graphene Fiber through Sequential Interfacial Interactions, ACS Nano 12 (9) (2018) 8901–8908, https://doi.org/10.1021/acsnano.8b04322.

[33] Sung Min Kang, Sungjin Park, Daewon Kim, Sung Young Park, Rodney S. Ruoff, Haeshin Lee, Simultaneous reduction and surface functionalization of graphene oxide by mussel-inspired chemistry, Adv. Funct. Mater. 21 (1) (2011) 108–112, https://doi.org/10.1002/adfm.201001692.

[34] J.H. Waite, M.L. Tanzer, Polyphenolic substance of mytilus edulis: novel adhesive containing L-dopa and hydroxyproline, Science 212 (1981) 1038–1040.

[35] Sabrina Schindler, Thomas Bechtold, Mechanistic insights into the electrochemical oxidation of dopamine by cyclic voltammetry, J. Electroanal. Chem. 836 (2019) 94–101, https://doi.org/10.1016/j.jelechem.2019.01.069.

[36] Sabrina Schindler, Noemí Aguiló-Aguayo, Urs Dornbierer, Thomas Bechtold, Anodic coating of 1.4622 stainless steel with polydopamine by repetitive cyclic voltammetry and galvanostatic deposition, Ind. Eng. Chem. Res. 59 (1) (2020) 236–244, https://doi.org/10.1021/acs.iecr.9b05603.s001.

[37] A.K. Das, M. Srivastav, R.K. Layek, M.E. Uddin, D. Jung, N.H. Kim, J.H. Lee, Iodide-mediated room temperature reduction of graphene oxide: a rapid chemical route for the synthesis of a bifunctional electrocatalyst, J. Mater. Chem. A 2 (2014) 2055–2060.

[38] Sasha Stankovich, Dmitriy A. Dikin, Richard D. Piner, Kevin A. Kohlhaas, Alfred Kleinhammes, Yuanyuan Jia, Yue Wu, SonBinh T. Nguyen, Rodney S. Ruoff, Synthesis of graphene-based nanosheets via chemical reduction of exfoliated graphite oxide, Carbon 45 (7) (2007) 1558–1565, https://doi.org/10.1016/j.carbon.2007.02.034.

[39] D. Yang, S. Huang, M.N. Ruan, S.X. Li, J.W. Yang, Y.B. Wu, W.L. Guo, L.Q. Zhang, Mussel inspired modification for aluminium oxide/silicone elastomer composites with largely improved thermal conductivity and low dielectric constant, Ind. Eng. Chem. Res. 57 (2018) 3255–3262.

[40] Shengguo Zhou, Xiaobo Zhu, Liqiu Ma, Qingqing Yan, Shuncai Wang, Outstanding superhydrophobicity and corrosion resistance on carbon-based film surfaces coupled with multi-walled carbon nanotubes and nickel nano-particles, Surf. Sci. 677 (2018) 193–202, https://doi.org/10.1016/j.susc.2018.07.010.

[41] T. Liu, H. Zhao, J. Li, D. Zhang, L. Wang, POSS-tetraaniline based giant molecule: synthesis, self-assembly, and active corrosion protection of epoxy-based organic coatings, Corros. Sci. 168 (2020), 108555.

[42] B. Ramezanzadeh, S. Niroumandrad, A. Ahmadi, M. Mahdavian, M.H. Mohamadzadeh Moghadam, Enhancement of barrier and corrosion protection performance of an epoxy coating through wet transfer of amino functionalized graphene oxide, Corrosion Science 103 (2016) 283–304, https://doi.org/10.1016/j.corsci.2015.11.033.

[43] Emilio Cano, Diana Lafuente, David M. Bastidas, Use of EIS for the evaluation of the protective properties of coatings for metallic cultural heritage: a review, J Solid State Electrochem 14 (3) (2010) 381–391, https://doi.org/10.1007/s10008-009-0902-6.

[44] Jean-Baptiste Jorcin, Mark E. Orazem, Nadine Pébère, Bernard Tribollet, CPE analysis by local electrochemical impedance spectroscopy, Electrochimica Acta 51 (8-9) (2006) 1473–1479, https://doi.org/10.1016/j.electacta.2005.02.128.

[45] S.G. Zhou, X.B. Zhu, Q.Q. Yan, S.C. Wang, Corrosion resistance and self-cleaning behaviour of Ni/a-C: H superhydrophobic films, Surf. Eng. 34 (2018) 611–619.

[46] V.N. Nguyen, F.X. Perrin, J.L. Vernet, Water permeability of organic/inorganic hybrid coatings prepared by sol-gel method: a comparison between gravimetric and capacitance measurements and evaluation of non-Fickian sorption models, Corros. Sci. 47 (2005) 397–412.

[47] D.M. Brasher, A.H. Kingsbury, Electrical measurements in the study of immersed paint coatings on metal. I. Comparison between capacitance and gravimetric methods of estimating water-uptake, J. Chem. Technol. Biot 4 (2010) 62–72.

[48] María del Alamo-Sanza, Luis Miguel Cárcel, Ignacio Nevares, Characterization of the oxygen transmission rate of oak wood species used in cooperage, J. Agric. Food Chem. 65 (3) (2017) 648–655, https://doi.org/10.1021/acs.jafc.6b05188.

[49] V.D. Castro, S. Ciampi, XPS study of the growth and reactivity of FeMnO thin films, surf, sci. 331–333 (1995) 294–299.

[50] R. Elemuren, R. Evitts, I.N.A. Oguocha, G. Kennell, R. Gerspacher, A.G. Odeshi, Full factorial, microscopic and spectroscopic study of erosion-corrosion of AISI 1018 steel elbows in potash brine-sand slurry, Tribol. Int. 142 (2020), 105989.

[51] P. Colomban, S. Cherifi, G. Despert, Raman identification of corrosion products on automotive galvanized steel sheets, J. Raman Spectrosc. 39 (7) (2008) 881–886, https://doi.org/10.1002/jrs.1927.

[52] Xin Zhang, Kui Xiao, Chaofang Dong, Junsheng Wu, Xiaogang Li, Yizhong Huang, In situ Raman spectroscopy study of corrosion products on the surface of carbon steel in solution containing Cl− and, Eng. Failure Anal. 18 (8) (2011) 1981–1989, https://doi.org/10.1016/j.engfailanal.2011.03.007.

[53] S.J. Oh, D.C. Cook, H.E. Townsend, Characterization of iron oxides commonly formed as corrosion products on steel, Hyperfine Interact. 112 (1998) 59–66.

[54] S. Ramya, D. Nanda Gopala Krishna, U.K. Mudali, In-situ Raman and X-ray photoelectron spectroscopic studies on the pitting corrosion of modified 9Cr-1Mo steel in neutral chloride solution, Appl. Surf. Sci. 428 (2018) 1106–1118, https://doi.org/10.1016/j.apsusc.2017.09.179.

[55] D. Bersani, P.P. Lottici, A. Montenero, Micro-Raman investigation of iron oxide films and powders produced by sol-gel syntheses, J. Raman Spectrosc. 30 (5) (1999) 355–360, https://doi.org/10.1002/(SICI)1097-4555(199905)30:5<355::AID-JRS398>3.0.CO;2-C.

[56] Florence Mercier-Bion, Jiaying Li, Hélène Lotz, Ludovic Tortech, Delphine Neff, Philippe Dillmann, Electrical properties of iron corrosion layers formed in anoxic environments at the nanometer scale, Corros. Sci. 137 (2018) 98–110, https://doi.org/10.1016/j.corsci.2018.03.028.

[57] Sepideh Pourhashem, Mohammad Reza Vaezi, Alimorad Rashidi, Mohammad Reza Bagherzadeh, Exploring corrosion protection properties of solvent based epoxy-graphene oxide nanocomposite coatings on mild steel, Corros. Sci. 115 (2017) 78–92, https://doi.org/10.1016/j.corsci.2016.11.008.

[58] Yaya Li, Zhenzhen Yang, Hanxun Qiu, Yigang Dai, Qingbin Zheng, Jing Li, Junhe Yang, Self-aligned graphene as anticorrosive barrier in waterborne polyurethane composite coatings, J. Mater. Chem. A 2 (34) (2014) 14139–14145, https://doi.org/10.1039/C4TA02262A.

[59] Kai Qi, Yimin Sun, Hongwei Duan, Xingpeng Guo, A corrosion-protective coating based on a solution-processable polymer-grafted graphene oxide nanocomposite, Corros. Sci. 98 (2015) 500–506, https://doi.org/10.1016/j.corsci.2015.05.056.

[60] C. Liu, H. Zhao, P. Hou, B. Qian, X. Wang, C. Guo, L. Wang, Efficient graphene/cyclodextrin-based nanocontainer: synthesis and host-guest inclusion for self-healing anticorrosion application, ACS Appl. Mater. Interfaces 10 (2018) 36229–36239.